

Article

Effect of Mixing Intensity on Electrochemical Performance of Oxide/Sulfide Composite Electrolytes

Jessica Gerstenberg ^{1,2,*}, Dominik Steckermeier ^{1,2}, Arno Kwade ^{1,2} and Peter Michalowski ^{1,2}

¹ Institute for Particle Technology, Technische Universität Braunschweig, 38104 Braunschweig, Germany

² Battery LabFactory Braunschweig, Technische Universität Braunschweig, 38106 Braunschweig, Germany

* Correspondence: j.gerstenberg@tu-braunschweig.de

Abstract: Despite the variety of solid electrolytes available, no single solid electrolyte has been found that meets all the requirements of the successor technology of lithium-ion batteries in an optimum way. However, composite hybrid electrolytes that combine the desired properties such as high ionic conductivity or stability against lithium are promising. The addition of conductive oxide fillers to sulfide solid electrolytes has been reported to increase ionic conductivity and improve stability relative to the individual electrolytes, but the influence of the mixing process to create composite electrolytes has not been investigated. Here, we investigate Li₃PS₄ (LPS) and Li₇La₃Zr₂O₁₂ (LLZO) composite electrolytes using electrochemical impedance spectroscopy and distribution of relaxation times. The distinction between sulfide bulk and grain boundary polarization processes is possible with the methods used at temperatures below 10 °C. We propose lithium transport through the space-charge layer within the sulfide electrolyte, which increases the conductivity. With increasing mixing intensities in a high-energy ball mill, we show an overlay of the enhanced lithium-ion transport with the structural change of the sulfide matrix component, which increases the ionic conductivity of LPS from 4.1×10^{-5} S cm⁻¹ to 1.7×10^{-4} S cm⁻¹.



Citation: Gerstenberg, J.; Steckermeier, D.; Kwade, A.; Michalowski, P. Effect of Mixing Intensity on Electrochemical Performance of Oxide/Sulfide Composite Electrolytes. *Batteries* **2024**, *10*, 95. <https://doi.org/10.3390/batteries10030095>

Academic Editors: Claudio Gerbaldi and Catia Arbizzani

Received: 30 January 2024

Revised: 1 March 2024

Accepted: 5 March 2024

Published: 7 March 2024



Copyright: © 2024 by the authors. Licensee MDPI, Basel, Switzerland. This article is an open access article distributed under the terms and conditions of the Creative Commons Attribution (CC BY) license (<https://creativecommons.org/licenses/by/4.0/>).

Keywords: solid-state battery; hybrid solid electrolyte; space-charge layer; distribution of relaxation times; LPS; LLZO

1. Introduction

All-solid-state batteries (ASSBs) offer the potential for enhanced safety and energy density in comparison to the current state-of-the-art liquid electrolyte lithium-ion batteries (LIBs) [1]. LIBs, which are commonly used to power portable electronic devices and electric vehicles, are reaching their limits in meeting the requirements for energy and power density, as well as safety concerns [2]. ASSBs aim to utilize metallic lithium as an anode material, thereby increasing the energy density when compared to conventional graphite anodes [3]. This is achieved by replacing the liquid electrolyte with a solid electrolyte (SE) and utilizing high-voltage cathode materials [4]. SEs demonstrate low self-discharge, excellent thermal stability, high ionic conductivities, and favorable chemical properties [5–7]. Two categories of SEs are being investigated for their application in ASSBs: solid polymer materials and inorganic materials. The most important organic SEs are sulfide (e.g., thiophosphate) and oxide electrolytes. These distinct material classes exhibit various advantages and disadvantages. Sulfide electrolytes such as Li₃PS₄ (LPS) possess high ionic conductivity, a good electrochemical stability, and easy processability, but form H₂S when exposed to moisture and suffer from an unstable interface with the lithium anode [8–10]. Oxide electrolytes, such as the garnet Li₇La₃Zr₂O₁₂ (LLZO), exhibit high ionic conductivity and electrochemical stability, but have poor interfacial compatibility with metallic lithium and require high processing temperatures (sintering). Consequently, oxide SEs are disadvantageous for use in cathodes due to the degradation of the active material at elevated temperatures [11–13]. The mechanical flexibility of SEs, as determined

by their elastic modulus, is crucial for their performance, as the volume expansion during cycling can lead to electrode cracking [14]. While a single type of SE that possesses all the necessary properties to address current challenges has not been discovered, the focus on hybrid systems is increasing [15,16].

Inorganic solid electrolytes facilitate ion migration through crystal defects or special crystal structures. Excitation of ordered lattice ions leads to their movement to disordered neighboring sites, enabling collective diffusion through the electrolyte [17]. In glass-ceramic sulfide solid electrolytes, the replacement of oxygen elements with sulfur expands the original ion radius, thus enhancing the ion transport channels for lithium [18]. Li₃PS₄ is a glassy sulfide solid electrolyte with relatively high ionic conductivity, depending on the synthesis method. Mechanical synthesis has shown competitive conductivities ranging from 2×10^{-4} S cm⁻¹ [19] to 3×10^{-3} S cm⁻¹ [20] at room temperature. 70Li₂S-30P₂S₂ glasses, prepared by milling or cold-pressing followed by treatment to reach the glass transition temperature, exhibit high ionic conductivities of up to 3×10^{-3} S cm⁻¹ [21] and 1.7×10^{-2} S cm⁻¹ [22]. The improvement of lithium conduction in Li₂S-P₂S₂ glasses can be achieved on a microscopic level by reducing the grain boundary resistance between particles and on a macroscopic level by decreasing the pellet density [23,24].

The addition of filler particles to a thiophosphate SE can lead to an increase in conductivity due to the formation of space-charge layers, increased dislocation density, or the formation of new phases [25]. The theory of space-charge layer formation proposed by Maier [26] is considered “generally acceptable” [17]: The interface or grain boundary of two materials is charged due to the different electrochemical potentials of both sides. While the bulk is charge neutral due to locally equal cation and anion defects (even with different formation enthalpies), the concentration of cation and anion defects at the two-material interface can be different, resulting in a space-charge layer. The addition of oxide fillers such as Li₇La₃Zr₂O₁₂ (LLZO), Al₂O₃, SiO₂, or Li₆ZnNb₄O₁₄ to β-Li₃PS₄ (LPS) could increase the conductivity of the thiophosphate SE [27,28]. Depending on the filler and particle size, the concentration to improve lithium-ion conductivity varies between 2 and 30 wt.-%. Composite electrolytes also refine the interfacial resistance with the metallic lithium anode and avoid sintering processes.

2. Materials and Methods

Handling of materials was performed in an argon-filled glovebox to prevent reaction with oxygen and water. All materials were used as received. The solid electrolytes Li₃PS₄ (LPS) from NEI Corporation, Somerset, NJ, USA, with a medium particle size of 3 to 5 μm and Li₇La₃Zr₂O₁₂ (LLZO) from SCHOTT AG, Mainz, Germany, with a medium particle size of 1 μm were mixed in different ratios in a high-energy ball mill (Emax, Retsch GmbH, Haan, Germany) combined with an external cooling aggregate (10 °C working temperature). Powders were processed in ZrO₂-lined jars with 125 mL volume and ZrO₂ grinding media (Tosoh Europe B.V., Amsterdam, The Netherlands) with 1 mm and 10 mm diameter at 400 rpm and 600 rpm rotational speed at 0.3 media-filling ratio for varying process times. The manufacturer specifies the conductivity of LPS as 10^{-4} to 10^{-5} S cm⁻¹, where the wide range is due to the different compaction and measurement parameters of the samples.

Raman spectroscopy (Alpha 300R, WITec GmbH, Kropfach, Germany) was conducted according to the method described by Hofer and Grube et al. [20] exciting samples at 532 nm in the range of 55 to 1555 cm⁻¹ and calculating a relative phase ratio of PS₄, P₂S₆, and P₂S₇. XRD was obtained using a diffractometer with a Cu Kα ($\lambda = 0.154$ nm) monochromatic source (Empyrean, Malvern Panalytical, Kassel, Germany) using an angular range of 5° to 120° 2θ with a step size of 0.05° 2θ. The samples were prepared in argon atmosphere and covered with Kapton foil to prevent exposure to air. All XRD measurement data are corrected by means of a reference spectrum of an unloaded sample holder. The reflexes were assigned to reference pattern 98-003-5018 of the ICSD database. The morphology of the samples was analyzed using a Desktop-SEM (Phenom XL, ThermoFisher Scientific Inc., Waltham, MA, USA).

The electrochemical tests were carried out in a measuring cell using two stainless steel plungers with a diameter of 16 mm as ion-blocking electrodes inserted into a Teflon cell as described in detail in [29]. The ball-milled powders forming the composite separator were processed into pellets by uniaxial pressing at 200 MPa in a two-column laboratory press (PW 10, P/O/Weber Laborpresstechnik, Remshalden, Germany). EIS was conducted at 40 MPa uniaxial pressure using a potentiostat (Zennium, Zahner-Elektrik GmbH & Co. KG, Kronach, Germany) at frequencies from 4 MHz to 10 Hz with an amplitude of 30 to 50 mV. The ionic conductivity is calculated by $\sigma_{\text{ion}} = l/(R A)$, with l being the sample thickness, R the resistance determined by EIS modeling, and A the sample area. With a minimum of three cells, EIS spectra were evaluated by distribution of relaxation times (DRT) by the method described at length by Heins et al. [30] with DRTtools software provided by Wan et al. [31]. With a minimum of three cells, the critical current density (CCD) was determined using a CTS LAB system (BaSyTec GmbH, Asselfingen, Germany) with symmetrical Li-SE-Li cells by stripping and deposition lithium at current densities ranging from 10 to 350 $\mu\text{A cm}^{-2}$ followed by an optional procedure ranging from 100 to 800 $\mu\text{A cm}^{-2}$ at a pressure of 20 MPa, where the failure step is indicating the CCD.

3. Results and Discussion

3.1. Quantification of the Polarization Processes within the Hybrid Separator

The ionic conductivity of solid electrolytes is characterized by transport processes within the bulk SE particles and across the particle interface between SE particles (commonly referred to as the grain boundary). For Li_3PS_4 , these two transport pathways are not easily separated by means of impedance spectroscopy [32]. EIS measures the overall reaction of a complex electrochemical system, with each process contributing to the resulting spectrum. Describing this reaction with an appropriate electrochemical model can be challenging when the different processes have similar time constants. However, DRT allows the estimation of time characteristics of an electrochemical system, typically using the Tikhonov regularization [30,31]. After pre-processing of the experimental impedance data according to Heins et al. [30], a regularization parameter λ of 10^{-5} was used to deconvolute the EIS spectra, resulting in the DRT spectra shown in Figure 1a. The corresponding Nyquist plots are displayed in Figure S1a of the Supplementary Materials. In comparison to Li_3PS_4 , for 70Li₂S-30P₂S₅ samples [22], Li₁₀SnP₂S₁₂ [33], or Li₁₀Si_{0.3}Sn_{0.7}P₂S₁₂ [34], it is typically easier to distinguish between two semicircles at low temperatures in high and low frequency regions that can be matched with bulk and grain boundary responses, respectively. The impedance spectra and the corresponding DRT plot of LPS show a single polarization process above 10 °C that can be attributed to both the bulk as well as the grain boundary transport (total). The process resistance corresponds to the area under the curve. The activation energy E_a from the Arrhenius plots shown in Figure 1b for the total polarization process is 0.45 eV above 10 °C and 0.5 eV below 10 °C, this minor deviation is caused by the limited data points. At lower temperatures, DRT analysis shows two polarization processes: here, we can separate the bulk and grain boundary process with an E_a of 0.34 eV and 0.58 eV, respectively. The similarity of the grain boundary activation energy below 10 °C and the total activation energy above 10 °C of 0.5 eV suggests that the transport process at higher temperatures is determined by the quality of the particle–particle contact in the pellet. The E_a for the total resistance of β -Li₃PS₄ is comparable to values found in the literature, varying from 0.29 eV [35] to 0.41 eV [36] and 0.47 eV [37].

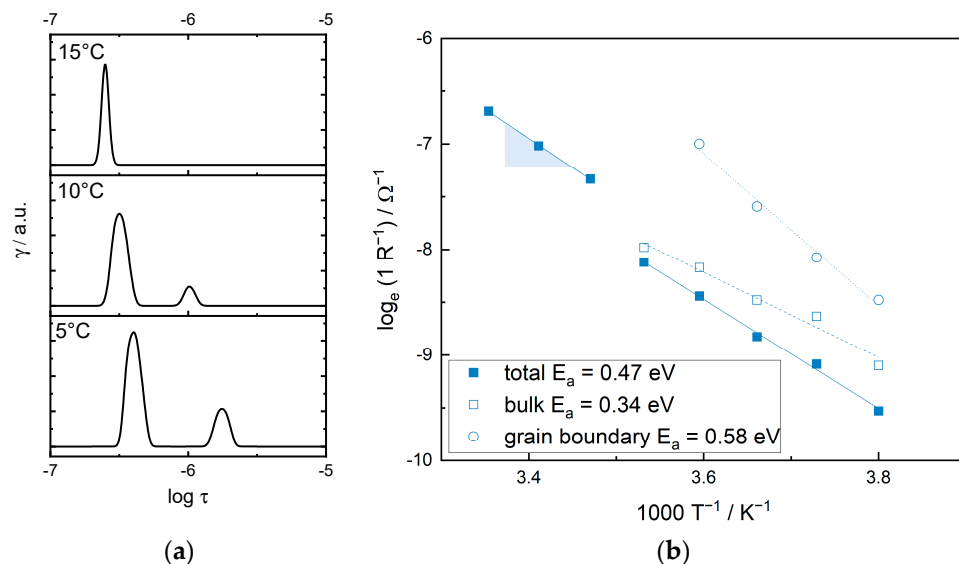


Figure 1. Transport properties of β -Li₃PS₄: (a) DRT plots of impedance and corresponding Arrhenius plots measured at different temperatures; (b) Arrhenius plot extracted from impedance data measured between -10 and 25 $^{\circ}\text{C}$, separated into bulk and grain boundary transport process as well as total transport below 10 $^{\circ}\text{C}$.

In order to evaluate the transport processes in an LPS–LLZO hybrid solid electrolyte, EIS measurements of the varying filler contents of LLZO in LPS were analyzed via DRT method. The results of 0 wt.-%, 30 wt.-%, and 60 wt.-% LLZO after 5 min milling time are shown in Figure 2. The corresponding Nyquist plots are displayed in Figure S1b of the Supplementary Materials. All samples up to 30 wt.-% filler are characterized by one process at 20 $^{\circ}\text{C}$ and two processes at 10 $^{\circ}\text{C}$, suggesting that the hybrid inhibits the same characteristic lithium transport pathways as the sulfide electrolyte. The corresponding E_a of 0.3 eV and 0.6 eV in both systems proposes bulk as well as grain boundary transport. With more than 40 wt.-% LLZO (results not shown), additional processes are quantifiable, i.e., three polarization processes appear for a 60 wt.-% hybrid electrolyte in Figure 2. The time constants as well as activation energies of these processes suggest bulk and grain boundary resistances as well as a third process. In the Supplementary Materials, Figure S2 shows the Arrhenius plots for a hybrid electrolyte with 60 wt.-% filler mixed for 30 min. Here, the attributed activation energies of 0.34 eV, 0.6 eV, and 0.47 eV corresponding, respectively, to the bulk and grain boundary processes of LPS and the LPS–LLZO interface, as described by Hüttl et al. [35], can be identified (Figure 3). Therefore, the ceramic electrolyte filler is adding an additional polarization process within the electrolyte pellet highly dependent on the system temperature and the filler content. The temperature dependence of the transportation processes is not visible at sufficiently high temperatures due to low activation barriers. Although low filler amounts show the same characteristic transportation processes as the sulfide matrix material, the hybrid electrolyte inhibits a lower resistance (corresponding to the peak area) than the sulfide electrolyte, suggesting the formation of a space-charge layer at the oxide–sulfide boundary.

3.2. Impact of Filler Particles on Ionic Conductivity

As LLZO is an oxide crystal, the high ionic conductivities of dense pellets above 0.1 mS/cm for 100 wt.-% LLZO are achieved by sintering at temperatures exceeding 1000 $^{\circ}\text{C}$ (Supplementary Materials Figure S3) [38,39]. The LPS–LLZO hybrid electrolytes on the other hand can be processed at room temperature, similar to the pure sulfide based solid electrolytes, due to the soft and dense character of the sulfide matrix in which the LLZO particles are embedded. For low mixing times of 5 min, Figure 4 shows that compared to the LPS electrolyte, embedding LLZO filler particles enhances the ionic conductivity

slightly. At a measuring temperature of 20 °C the conductivity exhibits a maximum at 30 wt.-% filler in LPS.

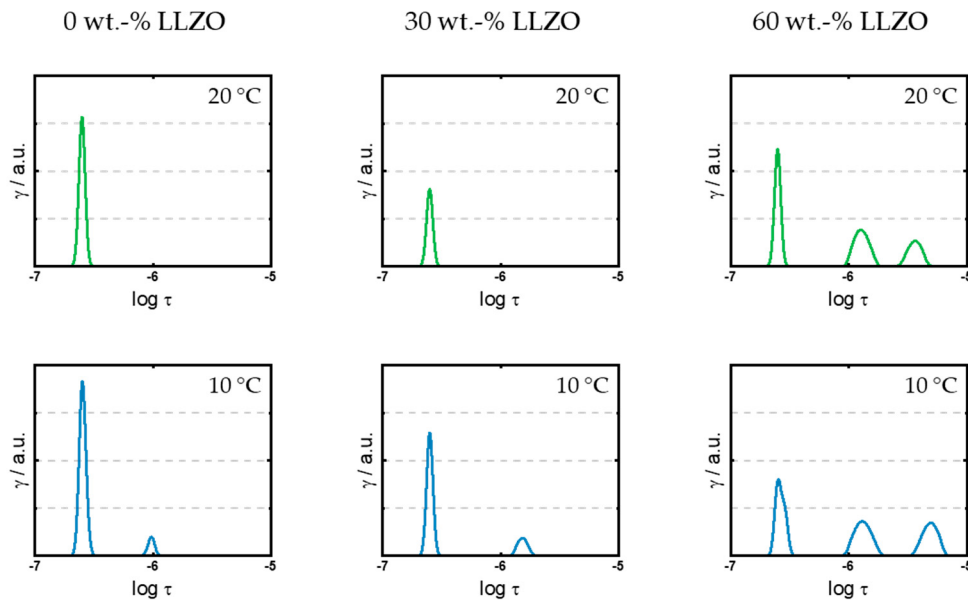


Figure 2. The polarization processes of a hybrid electrolyte validated via DRT at different filler contents of LLZO in an LPS electrolyte (mixing time of 5 min). In the hybrid electrolyte, the process at a lower relaxation time is characterized by an activation energy of 0.35 eV, while the second process at a higher relaxation time inhibits an activation energy of 0.85 eV.

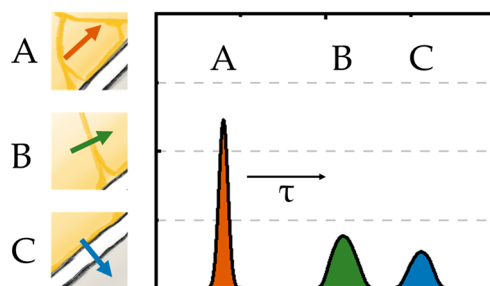


Figure 3. Lithium-ion transport processes in LPS–LLZO hybrid solid electrolyte with increasing time constants. (A) LPS bulk transport, (B) LPS grain boundary transport, (C) LPS-LLZO interface.

In consideration of the polarization processes analyzed by DRT, the lithium transport within the hybrid electrolyte is strongly affected by the LPS–LLZO interface at high filler contents. Increasing the amount of filler particles increases the interface between both materials and inhibits the pathways in the LPS matrix. This behavior is attributed to the blocking behavior of particles within a matrix as discussed by Hood et al. [28]. At lower filler contents, the space-charge effect exceeds the blocking effect resulting in an enhancement of ionic conductivity. Gao et al. stated that the conductivity is enhanced by space-charge effects at surfaces or internal boundaries as long as neighboring space-charge zones are well separated [17]. Derived from Maier's percolation model, agglomeration of filler particles or a high filler content will enable situations of space-charge layers overlapping or interfaces perceiving each other [26] resulting in a reduced conductivity of hybrid electrolytes at high filler contents.

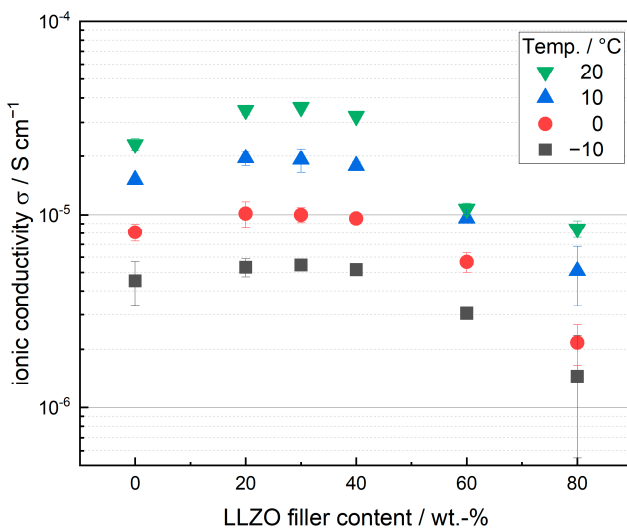


Figure 4. Ionic conductivity of LPS hybrid electrolyte pellets with different LLZO filler contents processed by high-energy ball milling for 5 min with ZrO_2 grinding media with 10 mm diameter at 400 rpm rotational speed. EIS measuring temperature varied between $-10\text{ }^\circ\text{C}$ and $20\text{ }^\circ\text{C}$. Lithium-ion transport shows optimal filler content in LPS of 30 wt.-% at elevated measuring temperature.

Rangasamy et al. reported the same optimum filler content of 30 wt.-% for a conductivity enhancement from $1.6 \times 10^{-4} \text{ S cm}^{-1}$ to $5.36 \times 10^{-4} \text{ S cm}^{-1}$ [27]. However, the effect of the filler was greater than the impact measured at for 5 min mixing time in this study. Specifically, the ionic conductivity increased from $2.3 \times 10^{-5} \text{ S cm}^{-1}$ in LPS to $3.6 \times 10^{-5} \text{ S cm}^{-1}$ with 30 wt.-% LLZO in LPS. The lithium-ion conduction in the space-charge layer is highly dependent on the charge-carrier concentration as well as the specific atomic configuration [40]. When two different materials (i.e., sulfide and oxide) are in contact, the space-charge layer is dependent on the chemical potential difference between them [41–45]. The contact area inhibits a large interfacial resistance, making the effect unfavorable when using oxide cathode active materials and sulfide solid electrolytes. For example, for $\text{Li}_6\text{PS}_5\text{Cl}$ and LiCoO_2 , the interface is in Li^+ equilibrium because of the formation of a deficiency region on the sulfide electrolyte side and a Li^+ enriched positive charge density region on the oxide electrode [41,42]. While the Li^+ deficiency region in sulfides is unfavorable for interfaces between electrolyte and electrode materials, it enhances the lithium conductivity in the hybrid electrolytes investigated here. Space-charge layers also occur at the grain boundaries of particles made of the same material (such as solid electrolytes). In this case, the grain boundary core carries a negative charge, which generates nearby regions that are rich in lithium [40].

Since the optimum amount of filler particles shows no interface transport from LPS into LLZO in the DRT analysis, we propose an enhanced transport of lithium-ions in the Li^+ deficient negative charge density region on the sulfide side at the sulfide–oxide material boundary, presented in Figure 5a. Since an ion distribution occurs due to the different lithium chemical potentials [46], filler particles are usually ion-conducting (i.e., solid electrolytes) or allow lithium transport within their atomic structure (i.e., Al_2O_3 , SiO_2) [28]. The chemical potential is strongly affected by the dopants and the filler surface condition (i.e., carbonate layers on LLZO), explaining the differences in conductivity enhancement when comparing hybrid electrolyte literature. In hybrid electrolytes, the choice of filler for each matrix material should, therefore, be selected by its chemical potential. Figure 5b shows the effect of filler content on hybrid electrolyte conductivity, with the proposed transport mechanism in the region where the filler content is low enough for the space-charge layer to enhance lithium-ion transport. As the filler content increases, the system transitions to blocking conditions. Here, the carbonate layer on the LLZO particles may be responsible for the lower ion conduction when the ion is transported across the particle boundary [47,48].

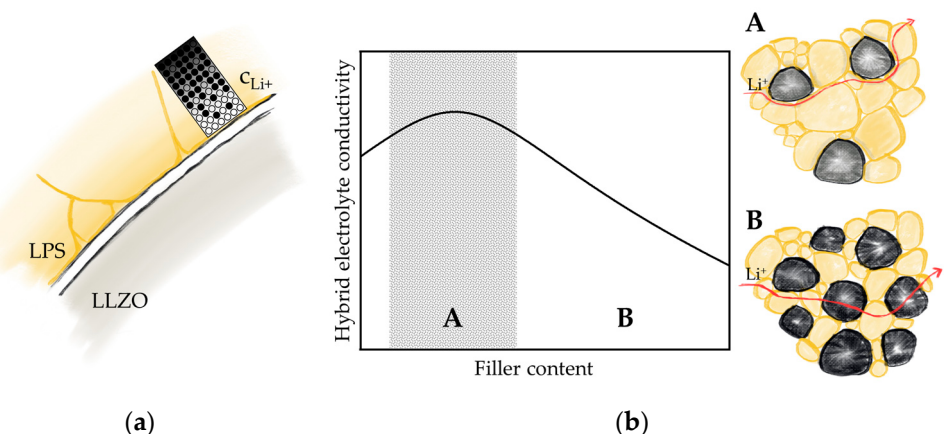


Figure 5. The theory of the lithium-ion transport (a) within the lithium deficient region of the space-charge layer between the LPS and LLZO material boundary and (b) the corresponding hybrid electrolyte conductivity. (A) Filler content low enough for the space-charge layer (lithium-ion depletion on the sulfide side of the sulfide–oxide interface) to enhance the electrolyte conductivity; (B) filler content with blocking conditions and lithium transport across the sulfide–oxide interface.

Reducing the measuring temperature lowers the positive effect of the filler particles resulting in only a slight increase in ionic conductivity below $0\text{ }^\circ\text{C}$. The thickness of the space-charge layer is proportional to the temperature [49], requiring a minimum temperature to take advantage of these hybrid systems.

The quantification of polarization processes and the ionic conductivity of LPS–LLZO hybrid electrolytes show that although the space-charge layer enhances the ion transport within the hybrid electrolyte, it has no polarization process detectable in DRT analysis. Instead, merely the transition to the ion transport across the particle boundary of LPS and LLZO can be detected by DRT. Nevertheless, this has an effect on the conductivity due to the increased resistance at the boundary of the two materials.

3.3. Impact of Optimized Mixing Parameters on Ionic Conductivity

Since the amount of energy introduced into the material by ball milling is highly dependent on the parameters, up to the point of chemical reactions through mechanochemical activation [50], we investigated the impact of the process parameters on the composite hybrid electrolyte powder. LPS as well as LPS with 30 wt.-% LLZO were processed with different rotational speeds, grinding media diameters, and milling times. The ionic conductivity of the process conducted at 600 rpm is presented in Figure 6a, while the results at 400 rpm rotational speed are shown in the Supplementary Materials in Figure S4. The ionic conductivities are also bundled in Table S1. The lithium conduction in the hybrid oxide–sulfide electrolyte is strongly dependent on the energy input during the process. Since the Emax high-energy mill has no measurement of the stressing conditions in the grinding chamber, Burmeister et al. described the increase in stressing energy with increasing media size diameter using the discrete element method [51]. Furthermore, longer milling times increase the number of stress events [52].

The use of small grinding media (diameter of 1 mm) at a low rotational speed of 400 rpm decreases the conductivity probably by creating a non-homogeneous composite, indicated by the high standard deviations. This is confirmed by the LLZO agglomerates visible in Figure S5 of the Supplementary Materials.

Increasing the stressing energy by larger zirconia balls or increased rotational speed leads to a slight but not significant increase in conductivity, probably due to the low mean stressing energy below 10^{-6} J [51]. The mean stressing energy can be enhanced to $6 \times 10^{-5}\text{ J}$ [51] with 10 mm grinding media size and 600 rpm rotational speed. Here, the composites show a significant increase in lithium-ion conductivity after 60 min milling

from $4.1 \times 10^{-5} \text{ S cm}^{-1}$ to $8.9 \times 10^{-5} \text{ S cm}^{-1}$ and $1.7 \times 10^{-4} \text{ S cm}^{-1}$ for 30 wt.-% LLZO filler in LPS and LPS, respectively.

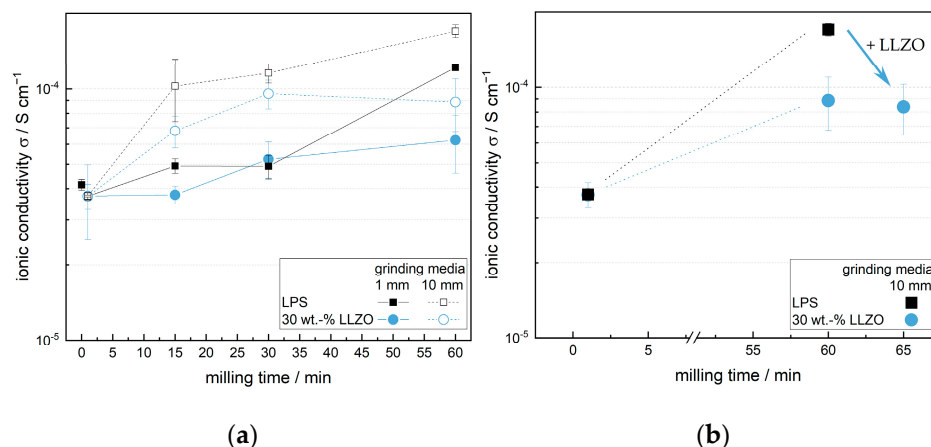


Figure 6. The ionic conductivity of LPS hybrid electrolyte pellets with 30 wt.-% LLZO filler content processed by high-energy ball milling with ZrO_2 grinding media varying in size at a rotational speed of 600 rpm. (a) Increasing the milling time has a significant influence on the lithium-ion transport within the electrolyte pellets. (b) The addition of LLZO into LPS processed for 60 min and mixing for an additional 5 min results in the same conductivity as the milling of both, LPS and LLZO, for a time of 60 min.

The oxide particles within the hybrid electrolyte will affect the energy input into the LPS particles during the milling process. To eliminate the possibility that the energy input into the matrix material (LPS) is responsible for the lower conductivity of the hybrid electrolyte, the filler particles were mixed into the sulfide electrolyte after it had been exposed to the mill for 60 min and mixed for another 5 min. As shown in Figure 6b, the addition of the LLZO particles after milling the LPS results in the same conductivity as milling the hybrid electrolyte for the same time.

The addition of filler in LPS also has an influence on the cycling behavior and critical current density (CCD) of the sulfide electrolytes [27,28,53]. In Figure 7, the CCD of LPS and 30 wt.-LLZO filler in LPS is plotted against the ionic conductivity of the electrolytes at varying milling times. Samples milled for 1 min with low ionic conductivities show a high CCD standard deviation, suggesting an inhomogeneous pellet structure, affecting the dendrite growth [54,55]. With sufficient milling time, the CCD shows a correlation with the ionic conductivity: both increasing with milling time. LPS milled for 60 min shows the best performance with regard to CCD and conductivity. The cycling data in Figure S6 of the Supplementary Materials also show a decreased resistance when comparing samples after 15 and 60 min milling time. While the CCD of LPS is in the range of reported values [56,57], it is not increased by the addition of filler particles.

The pellets exhibit a dense, homogeneous structure without agglomerates (Figure 8). The morphology of LPS in Figure 8a alters with the milling time suggesting a change in structure. This is supported by Raman analysis of the impurity phase after 1 min and 60 min milling as shown in Figure 9a, revealing a slightly increased proportion of the $[\text{PS}_4]^{3-}$ phase due to the energy input during milling. At the same time, the X-ray diffraction data in Figure 9b depicts a broadening and intensity decrease of reflections with milling time, proving the amorphization of the LPS matrix material within the process. Stöffler et al. have already established a similar relation, decreasing the crystalline character of the initial binary compounds Li_2S and P_2S_5 with increasing milling time [58]. Li_3PS_4 synthesized by ball milling usually has a higher ionic conductivity compared to the material obtained by liquid-phase synthesis, dependent on the polarity and crystallinity of the electrolyte [59,60]. Considering this, the increased ionic conductivity is a result of the structural change to lower crystallinity of the matrix LPS.

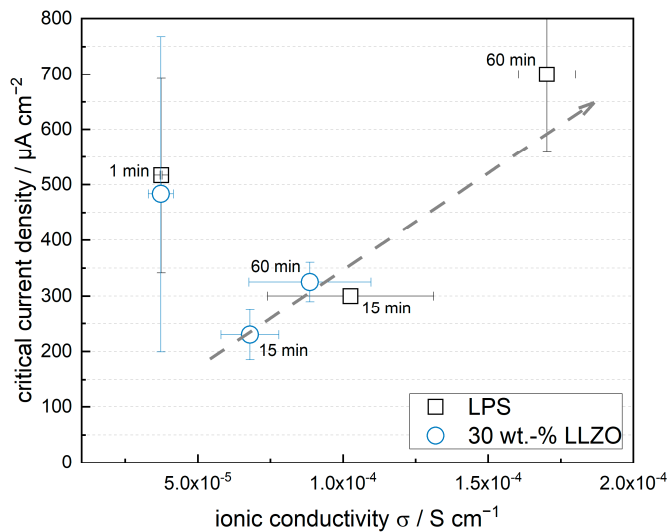


Figure 7. The critical current density and ionic conductivity of LPS hybrid electrolyte pellets with 30 wt.-% LLZO filler content processed by high-energy ball milling with ZrO_2 grinding media, with a size of 10 mm, at a rotational speed of 600 rpm. The corresponding milling times are indicated at the symbol. After 1 min milling time, the samples show a high CCD standard deviation and low ionic conductivities. At both the 15 and 60 min milling time, the samples are more homogeneous, and the CCD increases with increasing ionic conductivity (grey line).

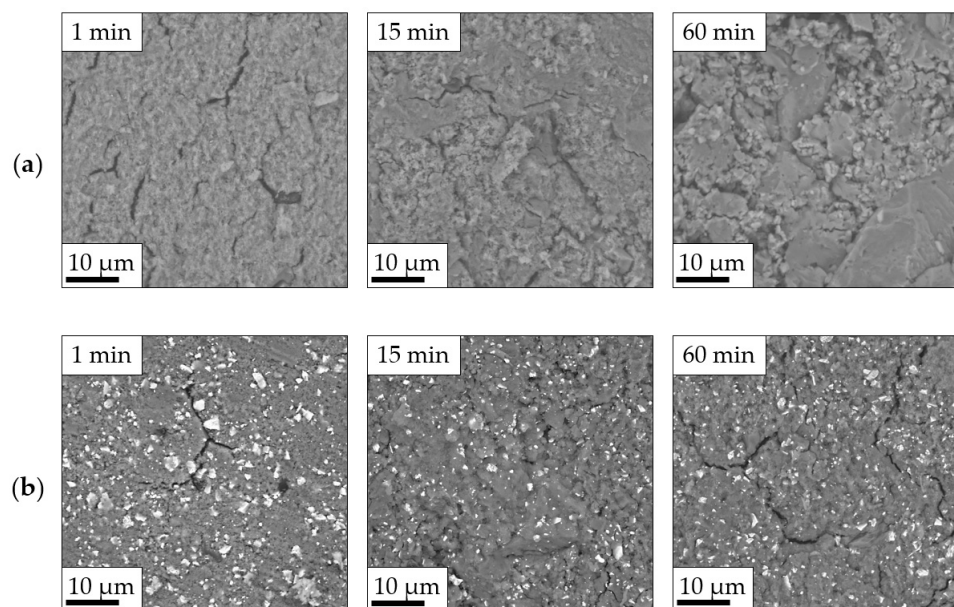


Figure 8. Top-view microstructure of (a) LPS separator pellets and (b) hybrid LPS with 30 wt.-% LLZO separator pellets processed by high-energy ball milling with 10 mm ZrO_2 grinding media at 600 rpm rotational speed displaying homogeneous distribution of matrix and filler particles (lighter spots) within pellet.

The conductivity of the hybrid electrolyte remains unaffected by the addition of filler particles, whether added at the beginning of the process or after amorphization of the LPS. This suggests that the conductivity occurs solely through the matrix material and that the oxide particles impede this volumetrically. Upon subtracting the LLZO content of 13.85 vol.-% (30 wt.-%), the theoretical conductivity increases slightly from approximately 0.8 mS cm^{-1} to a theoretical value of 0.95 mS cm^{-1} . Furthermore, filler particles alter the tortuosity of the matrix material. According to Kaiser et al. [61], an increase in effective tortuosity to approximately 1.5 with a sulfide content of 70% is conceivable. This increase,

in addition to volumetric inhibition, would result in a theoretical conductivity of the hybrid electrolyte of 1.4 mS cm^{-1} , which falls within the range of the LPS measured with 1.7 mS cm^{-1} . The use of filler particles in modified LPS, which has been amorphized by ball milling, is simply a geometric obstruction.

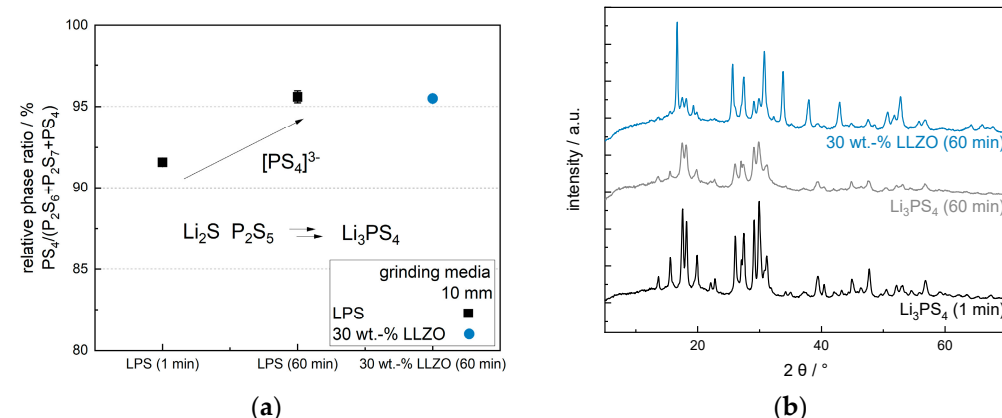


Figure 9. The impact of the milling process (10 mm grinding media, 600 rpm, 60 min) on the hybrid solid electrolyte. (a) The relative phase ratio of impurity phases in the Li_3PS_4 phase of LPS and hybrid electrolytes and (b) the X-ray diffraction spectra of LPS and hybrid electrolytes.

The literature indicates that optimal filler proportions vary depending on the sulfides and filler material used. In Figure 10, the conductivity of the hybrid electrolytes is plotted against the filler proportions after 60 min mixing time to eliminate the possibility that the amorphization of the LPS shifts the optimum filler proportion. Nonetheless, the lithium-ion conductivity of LLZO proportions between 10 and 30 vol.-% is comparable and lower than that of milled LPS. The design of hybrid electrolytes is crucial for optimized ion transport as it determines the formation of the space-charge layer. The combination of materials used plays a significant role in this process. The change in the matrix material (LPS) by milling may have an impact on the SCL, which should be taken into consideration. The ionic conductivities of the varying milling times and LLZO filler contents are bundled in Table S1.

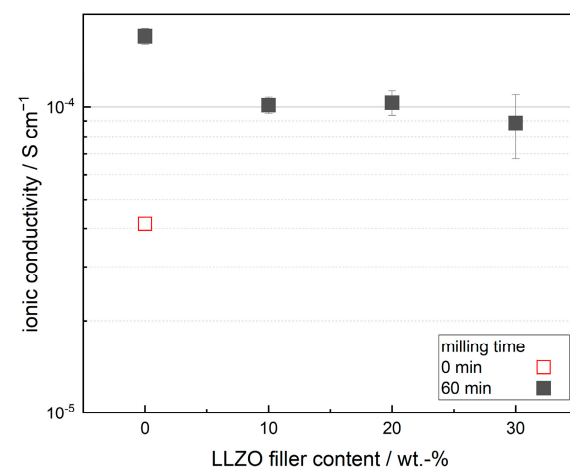


Figure 10. Ionic conductivity of LPS hybrid electrolyte pellets with different LLZO filler contents processed by high-energy ball milling for 60 min with ZrO_2 grinding media with 10 mm diameter at 600 rpm rotational speed. EIS measuring temperature was kept constant at 25°C . The lithium-ion transport properties of LPS are improved by milling process compared to LPS used as received (0 min). The ionic conductivity shows optimally without any LLZO filler addition.

4. Conclusions

Our study contributes significant insights into the ongoing debate regarding the efficacy of ceramic fillers in sulfide solid electrolytes. We have demonstrated that while ceramic fillers like LLZO can enhance the performance of LPS-based composites, the outcome is highly dependent on the combination of materials and the specific surface conditions of the fillers. In such hybrid electrolytes, the space-charge effect introduces a lithium depletion zone on the sulfide side of the interface between the sulfide matrix and the oxide filler, increasing the transport through the electrolyte. We identified an optimum filler content of 30 wt.-% for LPS–LLZO hybrid electrolytes at low mixing times. With this amount of LLZO, the space-charge effect improves the lithium-ion transport within the hybrid system. Increasing the filler content further will enhance the blocking behavior by altering the transport, introducing an additional polarization process detectable in EIS measurements. This process could be associated with the lithium-ion transport across the LPS–LLZO interface.

Furthermore, our research highlights the significant role of the manufacturing process, particularly the frequently used ball milling, in determining the ionic conductivity of hybrid electrolytes. Introducing energy into the Li_3PS_4 sulfide matrix impacts the crystallinity of the material. This energy input is dependent on the mixing times and ball-milling parameters. The structural change of LPS has a significant impact on the lithium-ion transport in the investigated oxide/sulfide composite electrolytes. At the same time, the space-charge effect is influenced heavily by the amorphization of the sulfide. Introducing oxide fillers into a milled and thereby amorphous Li_3PS_4 sulfide matrix reduces the lithium-ion conductivity. The space-charge effect is overlaid by the structural change in LPS. The filler particles now present a geometric obstruction, changing the effective tortuosity.

Considering this, the hybrid electrolyte lithium-ion conductivity is highly dependent on the complex interplay between the composite components and the manufacturing process. In our study, the manufacturing process of the hybrid electrolyte had a considerably higher impact on the ionic conductivity than the space-charge or blocking effects. Future research should, thus, explore the optimization of the filler materials as well as the processing conditions to further enhance the performance of hybrid solid electrolytes.

Supplementary Materials: The following supporting information can be downloaded at: <https://www.mdpi.com/article/10.3390/batteries10030095/s1>.

Author Contributions: Conceptualization, Validation, Formal Analysis, Investigation, Writing—Original Draft Preparation, Writing—Review and Editing, J.G.; Validation, Writing—Review and Editing, D.S. and P.M., with support from A.K.; Supervision, Project Administration, Funding Acquisition, A.K and P.M. All authors have read and agreed to the published version of the manuscript.

Funding: The authors gratefully acknowledge the financial support by the Federal Ministry for Economic Affairs and Energy (BMWi) giving the base for the here-demonstrated results within the research project 3D-SSB (funding number 03XP0202F) as well as the European Climate, Infrastructure and Environment Executive Agency (CINEA) and the European Union under the Horizon Europe project ADVAGEN (Grant Agreement n° 101069743). Views and opinions expressed are, however, those of the authors only and do not necessarily reflect those of the European Union or CINEA. We would like to acknowledge the funding by the Deutsche Forschungsgemeinschaft (DFG, German Research Foundation) under Germany's Excellence Strategy—EXC 2163/1—Sustainable and Energy Efficient Aviation (project 390881007) and the financial support of the project Mobilise (grant number ZN3247) by the Ministry for Science and Culture of the State of Lower Saxony (MWK). We also acknowledge support by the Open Access Publication Funds of Technische Universität Braunschweig.

Data Availability Statement: The raw data supporting the conclusions of this article will be made available by the authors on request.

Acknowledgments: The authors would like to thank Nicolas Schlüter, Institute of Energy and Process Systems Engineering, Technische Universität Braunschweig, for their support; Michael Grube, Fraunhofer Institute for Surface Engineering and Thin Films IST, for the fruitful discussions about sulfide electrolyte synthesis and Raman analysis; and Rorik Herbst for the automation and data

evaluation of the impedance spectra. Finally, they would like to express their sincere thanks to their project partner Andreas Roters and the SCHOTT AG, as well as all participating colleagues for their valuable assistance.

Conflicts of Interest: The authors declare no conflicts of interest. The authors declare the use of Generative AI and AI-assisted technologies in the writing process: During the preparation of this work, the authors used GPT-4 (OpenAI) as well as DeepL (DeepL SE) to improve readability and clarity. The authors reviewed and edited the content after usage and take full responsibility for the content of the publication.

References

1. Zheng, F.; Kotobuki, M.; Song, S.; Lai, M.O.; Lu, L. Review on solid electrolytes for all-solid-state lithium-ion batteries. *J. Power Sources* **2018**, *389*, 198–213. [[CrossRef](#)]
2. Janek, J.; Zeier, W.G. A solid future for battery development. *Nat. Energy* **2016**, *1*, 1167. [[CrossRef](#)]
3. Placke, T.; Kloepsch, R.; Dühnen, S.; Winter, M. Lithium ion, lithium metal, and alternative rechargeable battery technologies: The odyssey for high energy density. *J. Solid. State Electrochem.* **2017**, *21*, 1939–1964. [[CrossRef](#)]
4. Niu, C.; Liu, D.; Lochala, J.A.; Anderson, C.S.; Cao, X.; Gross, M.E.; Xu, W.; Zhang, J.-G.; Whittingham, M.S.; Xiao, J.; et al. Balancing interfacial reactions to achieve long cycle life in high-energy lithium metal batteries. *Nat. Energy* **2021**, *6*, 723–732. [[CrossRef](#)]
5. Irfan, M.; Atif, M.; Yang, Z.; Zhang, W. Recent advances in high performance conducting solid polymer electrolytes for lithium-ion batteries. *J. Power Sources* **2020**, *486*, 229378. [[CrossRef](#)]
6. Asano, T.; Yubuchi, S.; Sakuda, A.; Hayashi, A.; Tatsumisago, M. Electronic and Ionic Conductivities of $\text{LiNi}_{1/3}\text{Mn}_{1/3}\text{Co}_{1/3}\text{O}_2\text{-Li}_3\text{PS}_4$ Positive Composite Electrodes for All-Solid-State Lithium Batteries. *J. Electrochem. Soc.* **2017**, *164*, A3960–A3963. [[CrossRef](#)]
7. Wu, C.; Lou, J.; Zhang, J.; Chen, Z.; Kakar, A.; Emley, B.; Ai, Q.; Guo, H.; Liang, Y.; Lou, J.; et al. Current status and future directions of all-solid-state batteries with lithium metal anodes, sulfide electrolytes, and layered transition metal oxide cathodes. *Nano Energy* **2021**, *87*, 106081. [[CrossRef](#)]
8. Lian, P.-J.; Zhao, B.-S.; Zhang, L.-Q.; Xu, N.; Wu, M.-T.; Gao, X.-P. Inorganic sulfide solid electrolytes for all-solid-state lithium secondary batteries. *J. Mater. Chem. A* **2019**, *7*, 20540–20557. [[CrossRef](#)]
9. Wang, S.; Zhang, W.; Chen, X.; Das, D.; Ruess, R.; Gautam, A.; Walther, F.; Ohno, S.; Koerver, R.; Zhang, Q.; et al. Influence of Crystallinity of Lithium Thiophosphate Solid Electrolytes on the Performance of Solid-State Batteries. *Adv. Energy Mater.* **2021**, *11*, 2100654. [[CrossRef](#)]
10. Zhang, Q.; Cao, D.; Ma, Y.; Natan, A.; Aurora, P.; Zhu, H. Sulfide-Based Solid-State Electrolytes: Synthesis, Stability, and Potential for All-Solid-State Batteries. *Adv. Mater.* **2019**, *31*, e1901131. [[CrossRef](#)] [[PubMed](#)]
11. Kim, Y.; Kim, D.; Bliem, R.; Vardar, G.; Waluyo, I.; Hunt, A.; Wright, J.T.; Katsoudas, J.P.; Yildiz, B. Thermally Driven Interfacial Degradation between $\text{Li}_7\text{La}_3\text{Zr}_2\text{O}_{12}$ Electrolyte and $\text{LiNi}_{0.6}\text{Mn}_{0.2}\text{Co}_{0.2}\text{O}_2$ Cathode. *Chem. Mater.* **2020**, *32*, 9531–9541. [[CrossRef](#)]
12. Miara, L.; Windmüller, A.; Tsai, C.-L.; Richards, W.D.; Ma, Q.; Uhlenbruck, S.; Guillou, O.; Ceder, G. About the Compatibility between High Voltage Spinel Cathode Materials and Solid Oxide Electrolytes as a Function of Temperature. *ACS Appl. Mater. Interfaces* **2016**, *8*, 26842–26850. [[CrossRef](#)] [[PubMed](#)]
13. Zhu, Y.; Connell, J.G.; Tepavcevic, S.; Zapol, P.; Garcia-Mendez, R.; Taylor, N.J.; Sakamoto, J.; Ingram, B.J.; Curtiss, L.A.; Freeland, J.W.; et al. Dopant-Dependent Stability of Garnet Solid Electrolyte Interfaces with Lithium Metal. *Adv. Energy Mater.* **2019**, *9*, 1803440. [[CrossRef](#)]
14. Ramakumar, S.; Deviannapoorani, C.; Dhivya, L.; Shankar, L.S.; Murugan, R. Lithium garnets: Synthesis, structure, Li + conductivity, Li + dynamics and applications. *Prog. Mater. Sci.* **2017**, *88*, 325–411. [[CrossRef](#)]
15. Feng, J.; Wang, L.; Chen, Y.; Wang, P.; Zhang, H.; He, X. PEO based polymer-ceramic hybrid solid electrolytes: A review. *Nano Converg.* **2021**, *8*, 1–12. [[CrossRef](#)]
16. Ji, X.; Zhang, Y.; Cao, M.; Gu, Q.; Wang, H.; Yu, J.; Guo, Z.-H.; Zhou, X. Advanced inorganic/polymer hybrid electrolytes for all-solid-state lithium batteries. *J. Adv. Ceram.* **2022**, *11*, 835–861. [[CrossRef](#)]
17. Gao, J.; Zhao, Y.-S.; Shi, S.-Q.; Li, H. Lithium-ion transport in inorganic solid state electrolyte. *Chin. Phys. B* **2016**, *25*, 018211. [[CrossRef](#)]
18. Minami, T.; Hayashi, A.; Tatsumisago, M. Preparation and characterization of lithium ion-conducting oxysulfide glasses. *Solid. State Ionics* **2000**, *136–137*, 1015–1023. [[CrossRef](#)]
19. Hayashi, A.; Hama, S.; Morimoto, H.; Tatsumisago, M.; Minami, T. Preparation of $\text{Li}_2\text{S-P}_2\text{S}_5$ Amorphous Solid Electrolytes by Mechanical Milling. *J. Am. Ceram. Soc.* **2001**, *84*, 477–479. [[CrossRef](#)]
20. Hofer, M.; Grube, M.; Burmeister, C.F.; Michalowski, P.; Zellmer, S.; Kwade, A. Effective mechanochemical synthesis of sulfide solid electrolyte Li_3PS_4 in a high energy ball mill by process investigation. *Adv. Powder Technol.* **2023**, *34*, 104004. [[CrossRef](#)]
21. Mizuno, F.; Hayashi, A.; Tadanaga, K.; Tatsumisago, M. New, Highly Ion-Conductive Crystals Precipitated from $\text{Li}_2\text{S-P}_2\text{S}_5$ Glasses. *Adv. Mater.* **2005**, *17*, 918–921. [[CrossRef](#)]
22. Seino, Y.; Ota, T.; Takada, K.; Hayashi, A.; Tatsumisago, M. A sulphide lithium super ion conductor is superior to liquid ion conductors for use in rechargeable batteries. *Energy Environ. Sci.* **2014**, *7*, 627–631. [[CrossRef](#)]

23. Lu, S.; Kosaka, F.; Shiotani, S.; Tsukasaki, H.; Mori, S.; Otomo, J. Optimization of lithium ion conductivity of $\text{Li}_2\text{S}-\text{P}_2\text{S}_5$ glass ceramics by microstructural control of crystallization kinetics. *Solid. State Ionics* **2021**, *362*, 115583. [[CrossRef](#)]
24. Garcia-Mendez, R.; Smith, J.G.; Neuefeind, J.C.; Siegel, D.J.; Sakamoto, J. Correlating Macro and Atomic Structure with Elastic Properties and Ionic Transport of Glassy $\text{Li}_2\text{S}-\text{P}_2\text{S}_5$ (LPS) Solid Electrolyte for Solid-State Li Metal Batteries. *Adv. Energy Mater.* **2020**, *10*, 7. [[CrossRef](#)]
25. Shahi, K.; Wagner, J. Anomalous ionic conduction in $\text{AgBr}-\text{AgI}$ mixed crystals and multiphase systems. *J. Phys. Chem. Solids* **1982**, *43*, 713–722. [[CrossRef](#)]
26. Maier, J. Control parameters for electrochemically relevant materials: The significance of size and complexity. *Faraday Discuss.* **2014**, *176*, 17–29. [[CrossRef](#)] [[PubMed](#)]
27. Rangasamy, E.; Sahu, G.; Keum, J.K.; Rondinone, A.J.; Dudney, N.J.; Liang, C. A high conductivity oxide–sulfide composite lithium superionic conductor. *J. Mater. Chem. A* **2014**, *2*, 4111–4116. [[CrossRef](#)]
28. Hood, Z.D.; Wang, H.; Li, Y.; Pandian, A.S.; Parans Paranthaman, M.; Liang, C. The “filler effect”: A study of solid oxide fillers with β - Li_3PS_4 for lithium conducting electrolytes. *Solid State Ion.* **2015**, *283*, 75–80. [[CrossRef](#)]
29. Batzer, M.; Voges, K.; Wang, W.; Michalowski, P.; Kwade, A. Systematic evaluation of materials and recipe for scalable processing of sulfide-based solid-state batteries. *Mater. Today Commun.* **2022**, *30*, 103189. [[CrossRef](#)]
30. Heins, T.P.; Schlüter, N.; Schröder, U. Electrode-Resolved Monitoring of the Ageing of Large-Scale Lithium-Ion Cells by using Electrochemical Impedance Spectroscopy. *ChemElectroChem* **2017**, *4*, 2921–2927. [[CrossRef](#)]
31. Wan, T.H.; Saccoccia, M.; Chen, C.; Ciucci, F. Influence of the Discretization Methods on the Distribution of Relaxation Times Deconvolution: Implementing Radial Basis Functions with DRTtools. *Electrochimica Acta* **2015**, *184*, 483–499. [[CrossRef](#)]
32. Ohno, S.; Banik, A.; Dewald, G.F.; Kraft, M.A.; Krauskopf, T.; Minafra, N.; Till, P.; Weiss, M.; Zeier, W.G. Materials design of ionic conductors for solid state batteries. *Prog. Energy* **2020**, *2*, 022001. [[CrossRef](#)]
33. Bron, P.; Johansson, S.; Zick, K.; der Guenne, J.S.A.; Dehnen, S.; Roling, B. $\text{Li}_{10}\text{SnP}_2\text{S}_{12}$: An Affordable Lithium Superionic Conductor. *J. Am. Chem. Soc.* **2013**, *135*, 15694–15697. [[CrossRef](#)] [[PubMed](#)]
34. Bron, P.; Dehnen, S.; Roling, B. $\text{Li}_{10}\text{Si}_{0.3}\text{Sn}_{0.7}\text{P}_2\text{S}_{12}$ —A low-cost and low-grain-boundary-resistance lithium superionic conductor. *J. Power Sources* **2016**, *329*, 530–535. [[CrossRef](#)]
35. Hüttl, J.; Seidl, C.; Auer, H.; Nikolowski, K.; Görne, A.L.; Arnold, M.; Heubner, C.; Wolter, M.; Michaelis, A. Ultra-low LPS/LLZO interfacial resistance—Towards stable hybrid solid-state batteries with Li-metal anodes. *Energy Storage Mater.* **2021**, *40*, 259–267. [[CrossRef](#)]
36. de Klerk, N.J.J.; van der Maas, E.; Wagemaker, M. Analysis of Diffusion in Solid-State Electrolytes through MD Simulations, Improvement of the Li-Ion Conductivity in β - Li_3PS_4 as an Example. *ACS Appl. Energy Mater.* **2018**, *1*, 3230–3242. [[CrossRef](#)]
37. Ghidiu, M.; Schlem, R.; Zeier, W.G. Pyridine Complexes as Tailored Precursors for Rapid Synthesis of Thiophosphate Superionic Conductors. *Batter. Supercaps* **2021**, *4*, 607–611. [[CrossRef](#)]
38. Samsinger, R.F.; Schopf, S.O.; Schuhmacher, J.; Treis, P.; Schneider, M.; Roters, A.; Kwade, A. Influence of the Processing on the Ionic Conductivity of Solid-State Hybrid Electrolytes Based on Glass-Ceramic Particles Dispersed in PEO with LiTFSI. *J. Electrochem. Soc.* **2020**, *167*, 120538. [[CrossRef](#)]
39. Duan, H.; Zheng, H.; Zhou, Y.; Xu, B.; Liu, H. Stability of garnet-type Li ion conductors: An overview. *Solid. State Ionics* **2018**, *318*, 45–53. [[CrossRef](#)]
40. Gu, Z.; Ma, J.; Zhu, F.; Liu, T.; Wang, K.; Nan, C.-W.; Li, Z.; Ma, C. Atomic-scale study clarifying the role of space-charge layers in a Li-ion-conducting solid electrolyte. *Nat. Commun.* **2023**, *14*, 1632. [[CrossRef](#)]
41. Wang, L.; Xie, R.; Chen, B.; Yu, X.; Ma, J.; Li, C.; Hu, Z.; Sun, X.; Xu, C.; Dong, S.; et al. In-situ visualization of the space-charge-layer effect on interfacial lithium-ion transport in all-solid-state batteries. *Nat. Commun.* **2020**, *11*, 5889. [[CrossRef](#)]
42. Takada, K.; Ohno, T.; Ohta, N.; Ohnishi, T.; Tanaka, Y. Positive and Negative Aspects of Interfaces in Solid-State Batteries. *ACS Energy Lett.* **2018**, *3*, 98–103. [[CrossRef](#)]
43. Takada, K.; Ohta, N.; Zhang, L.; Xu, X.; Hang, B.T.; Ohnishi, T.; Osada, M.; Sasaki, T. Interfacial phenomena in solid-state lithium battery with sulfide solid electrolyte. *Solid. State Ionics* **2012**, *225*, 594–597. [[CrossRef](#)]
44. Haruyama, J.; Sodeyama, K.; Han, L.; Takada, K.; Tateyama, Y. Space-Charge Layer Effect at Interface between Oxide Cathode and Sulfide Electrolyte in All-Solid-State Lithium-Ion Battery. *Chem. Mater.* **2014**, *26*, 4248–4255. [[CrossRef](#)]
45. Cheng, Z.; Liu, M.; Ganapathy, S.; Li, C.; Li, Z.; Zhang, X.; He, P.; Zhou, H.; Wagemaker, M. Revealing the Impact of Space-Charge Layers on the Li-Ion Transport in All-Solid-State Batteries. *Joule* **2020**, *4*, 1311–1323. [[CrossRef](#)]
46. Maier, J. Ionic conduction in space charge regions. *Prog. Solid State Chem.* **1995**, *23*, 171–263. [[CrossRef](#)]
47. Huo, H.; Li, X.; Sun, Y.; Lin, X.; Doyle-Davis, K.; Liang, J.; Gao, X.; Li, R.; Huang, H.; Guo, X.; et al. Li_2CO_3 effects: New insights into polymer/garnet electrolytes for dendrite-free solid lithium batteries. *Nano Energy* **2020**, *73*, 104836. [[CrossRef](#)]
48. Biao, J.; Han, B.; Cao, Y.; Li, Q.; Zhong, G.; Ma, J.; Chen, L.; Yang, K.; Mi, J.; Deng, Y.; et al. Inhibiting Formation and Reduction of Li_2CO_3 to LiCx at Grain Boundaries in Garnet Electrolytes to Prevent Li Penetration. *Adv. Mater.* **2023**, *35*, e2208951. [[CrossRef](#)]
49. Katzenmeier, L.; Carstensen, L.; Bandarenka, A.S. Li^+ Conductivity of Space Charge Layers Formed at Electrified Interfaces Between a Model Solid-State Electrolyte and Blocking Au-Electrodes. *ACS Appl. Mater. Interfaces* **2022**, *14*, 15811–15817. [[CrossRef](#)]
50. Schlem, R.; Burmeister, C.F.; Michalowski, P.; Ohno, S.; Dewald, G.F.; Kwade, A.; Zeier, W.G. Energy Storage Materials for Solid-State Batteries: Design by Mechanochemistry. *Adv. Energy Mater.* **2021**, *11*, 2101022. [[CrossRef](#)]

51. Burmeister, C.F.; Hofer, M.; Molaiyan, P.; Michalowski, P.; Kwade, A. Characterization of Stressing Conditions in a High Energy Ball Mill by Discrete Element Simulations. *Processes* **2022**, *10*, 692. [[CrossRef](#)]
52. Kwade, A. A Stressing Model for the Description and Optimization of Grinding Processes. *Chem. Eng. Technol.* **2003**, *26*, 199–205. [[CrossRef](#)]
53. Zou, C.; Yang, L.; Luo, K.; Tao, X.; Yi, L.; Liu, X.; Luo, Z.; Wang, X. Ionic conductivity and interfacial stability of Li₆PS₅Cl-Li_{6.5}La₃Zr_{1.5}Ta_{0.5}O₁₂ composite electrolyte. *J. Solid State Electrochem.* **2021**, *25*, 2513–2525. [[CrossRef](#)]
54. Diallo, M.S.; Shi, T.; Zhang, Y.; Peng, X.; Shozib, I.; Wang, Y.; Miara, L.J.; Scott, M.C.; Tu, Q.H.; Ceder, G. Effect of solid-electrolyte pellet density on failure of solid-state batteries. *Nat. Commun.* **2024**, *15*, 858. [[CrossRef](#)] [[PubMed](#)]
55. Lu, Y.; Zhao, C.-Z.; Yuan, H.; Cheng, X.-B.; Huang, J.-Q.; Zhang, Q. Critical Current Density in Solid-State Lithium Metal Batteries: Mechanism, Influences, and Strategies. *Adv. Funct. Mater.* **2021**, *31*, 479. [[CrossRef](#)]
56. Garcia-Mendez, R.; Mizuno, F.; Zhang, R.; Arthur, T.S.; Sakamoto, J. Effect of Processing Conditions of 75Li₂S-25P₂S₅ Solid Electrolyte on its DC Electrochemical Behavior. *Electrochim. Acta* **2017**, *237*, 144–151. [[CrossRef](#)]
57. Poudel, T.P.; Deck, M.J.; Wang, P.; Hu, Y.-Y. Transforming Li₃PS₄ Via Halide Incorporation: A Path to Improved Ionic Conductivity and Stability in All-Solid-State Batteries. *Adv. Funct. Mater.* **2024**, *34*, 299. [[CrossRef](#)]
58. Stöffler, H.; Zinkevich, T.; Yavuz, M.; Hansen, A.-L.; Knapp, M.; Bednarčík, J.; Randau, S.; Richter, F.H.; Janek, J.; Ehrenberg, H.; et al. Amorphous versus Crystalline Li₃PS₄: Local Structural Changes during Synthesis and Li Ion Mobility. *J. Phys. Chem. C* **2019**, *123*, 10280–10290. [[CrossRef](#)]
59. Yamamoto, K.; Yang, S.; Takahashi, M.; Ohara, K.; Uchiyama, T.; Watanabe, T.; Sakuda, A.; Hayashi, A.; Tatsumisago, M.; Muto, M.; et al. High Ionic Conductivity of Liquid-Phase-Synthesized Li₃PS₄ Solid Electrolyte, Comparable to That Obtained via Ball Milling. *ACS Appl. Energy Mater.* **2021**, *4*, 2275–2281. [[CrossRef](#)]
60. Self, E.C.; Hood, Z.D.; Brahmbhatt, T.; Delnick, F.M.; Meyer, H.M.; Yang, G.; Rupp, J.L.M.; Nanda, J. Solvent-Mediated Synthesis of Amorphous Li₃PS₄/Polyethylene Oxide Composite Solid Electrolytes with High Li⁺ Conductivity. *Chem. Mater.* **2020**, *32*, 8789–8797. [[CrossRef](#)]
61. Kaiser, N.; Spannenberger, S.; Schmitt, M.; Cronau, M.; Kato, Y.; Roling, B. Ion transport limitations in all-solid-state lithium battery electrodes containing a sulfide-based electrolyte. *J. Power Sources* **2018**, *396*, 175–181. [[CrossRef](#)]

Disclaimer/Publisher’s Note: The statements, opinions and data contained in all publications are solely those of the individual author(s) and contributor(s) and not of MDPI and/or the editor(s). MDPI and/or the editor(s) disclaim responsibility for any injury to people or property resulting from any ideas, methods, instructions or products referred to in the content.